COLORADO STATE
UNIVERSITY
FORT COLLINS, COLORADO
80521

department of electrical engineering

N 73 28715

A THIN POLYMER INSULATOR FOR JOSEPHSON

TUNNELING APPLICATIONS

CASE FILE
COPY

Final Report

July 1973

C. W. Wilmsen

Colorado State University

Department of Electrical Engineering

Fort Collins, Colorado   80521

A THIN POLYMER INSULATOR FOR JOSEPHSON

TUNNELING APPLICATIONS

Final Report

July 1973

C. W. Wilmsen

I. Introduction

The research conducted with the support of NASA Grant No. NGR 06-992-094 was concerned with three main areas:

a) Exploring the possibility of using a organic monolayer formed from a vapor as an insulating barrier for thin film Josephson junctions,

b) Experimentally investigating the effect of an organic monolayer on the transition temperature of a thin film superconductor, and

c) Analyzing the geometric factors which influence Josephson junctions and Josephson junction interferometers.

Most of the technical details of this research has already been presented in the six semi-annual progress reports. This final report summarizes and places in perspective these many details. Each of the three main research area will be discussed separately.

II. Organic Monolayers for Josephson Barriers

Brief summary

Pb - organic - Al junctions were formed which displayed Josephson characteristics. These junctions had approximately 1 ohm junction resistance at room temperature but the resistance increased with time when the junctions were stored in room air. The Josephson characteristics disappeared after aging. The cause of the aging is unknown. The organic layer was formed from a crucible containing stearoyl peroxide with the substrate heated to 175°C in a vacuum of approximately 10^{-6} Torr.

From these results it is concluded that Josephson barriers can be formed from an organic vapor and that the barrier is probably only a monolayer thick.
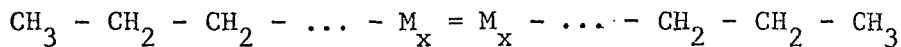
Formation of Organic Barriers

The original model for monolayer formation is as follows:

A thin film of superconducting metal is first deposited on a glass substrate in an ultra high vacuum. The ultra high vacuum reduces the possibility of oxidation of the metal surface before the organic reacts with the surface. After the superconductor is deposited, an organic vapor is introduced into the vacuum. The organic is a dimer molecule made up of two monomer molecules as shown in the figure.
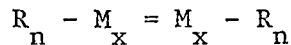
$$CH_3 - CH_2 - CH_2 - \ldots - M_x -$$
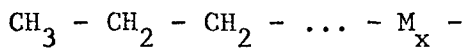
M_x is a reactive radical or polar group.

Monomer

$$CH_3 - CH_2 - CH_2 - \ldots - M_x = M_x - \ldots - CH_2 - CH_2 - CH_3$$

or

$$R_n - M_x = M_x - R_n$$

where R_n is a hydrocarbon chain of length n.

Dimer

The dimer must be broken up into two stable monomers which then react with the surface. The first layer of adsorbed monomers must be tightly bound to the metal surface while the succeeding layers are only weakly bound. This would allow heat to drive off all but the tightly bound first layer. Thus, a monolayer of the organic would be formed. The thickness of the layer would depend on the length of the hydrocarbon chain.

Basically, this model proved to be correct. However, there are a number of experimental difficulties which must be overcome in order to realize a Josephson barrier. These are
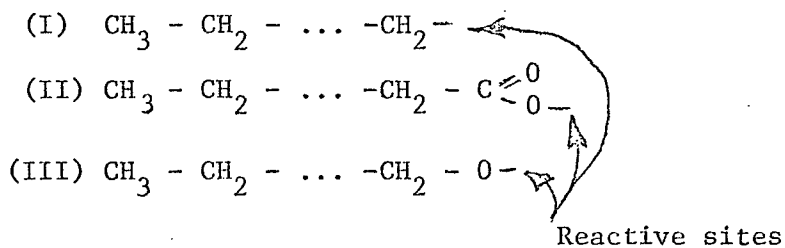
a) Determination of a suitable monomer

b) Synthesis of the dimer

c) Breaking the dimer bond

d) Driving off excess layers

e) Creating the organic vapor

Each of these will be discussed separately.

Determination of a suitable monomer

There are two important criteria in choosing the monomer. These

are that the monomer strongly attach to the metal film (40-100K cal/mole)

and that the monomer be stable, i.e. not decompose.

In order to determine, which monomer termination would bind

tightly to superconductors such as Pb and Sn we adapted a molecular

orbital energy program to the study of gas-solid surface reaction. This

work resulted in two publications $1,2$ which describe in detail both the cal-

culation method and the results. In brief, the calculations showed that

terminating groups which form an oxidative bond with surface will strongly

bond. This lead to the following monomers:

(I) $CH_3 - CH_2 - \ldots -CH_2 -$

(II) $CH_3 - CH_2 - \ldots -CH_2 - C\overset{\nearrow 0}{\underset{0 -}{}}$

(III) $CH_3 - CH_2 - \ldots -CH_2 - 0 -$

Reactive sites

Monomers I and III are stable while monomer II decomposes quite rapidly

$(10^{-9}$ sec) to

$$R_n - C\overset{\nearrow 0}{\underset{0 -}{\diagdown}} \longrightarrow R_n + CO_2$$
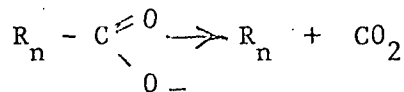
This means that in order to use monomer II, the dimer must be broken up
on the metal film surface.

Synthesis of the dimers

The synthesis of the dimers for monomers I and II was relatively
simple. The synthesis for monomer III was extremely difficult as was
carbon 14 labeled dimers for monomer II.

A serious attempt was made to label the No. II monomers with a
percentage of radioactive carbon 14 atom. This was tried in order to get
a quantitative measure of the surface coverage on the metal films. The
technique is relatively straight forward. The Pb is vacuum deposited and
the organic introduced. One carbon of the organic is radioactive; giving
off a 0.14 MeV electron. After exposing the Pb in the desired manner,
the system is opened and the Pb sample removed and placed in a counter.
The background count is substrated from the total count and compared with
the count expected from a monolayer. This technique could have provided
considerable data on the effect of the variation of deposition parameters
on the final film. Two problems arose to prevent successful completion of
this investigation. 1) The extreme cost of the labeled compounds and 2)
the radiation hazzard of conducting repeated tests.

A possible solution to the first problem is to synthesize the labeled
compounds from simpler and cheaper compounds. This proved too time consuming
and unreliable. We abandoned the C^{14} method in favor of a trial and error
approach to forming the monolayer.

Synthesis of the dimer for monomer III was also quite difficult primarily
due to decomposition of intermediate solutions and the poor mixing of the

long chain molecules. The details of the synthesis procedure are given in the February 1972 report. While this dimer was successfully synthesized, the amounts were small and rather impure.

Since dimer II proved to be usable for junction formation, we chose to concentrate on this more manageable organic.

Breaking the dimer band

Since the dimer is non-reactive, it must be broken up into two monomers. This can be done by heat, chemical reaction, an electron beam or by UV radiation. The chemical reaction method requires an additional chemical in the system which could cause problems. The electron beam and UV radiation could easily break many bonds within the monomer itself, and therefore spoil the monolayer formation. Heat on the other hand, is simple and effective.

To break up the dimer two methods of heating were tried: passing the dimer through a heated screen and heating the substrate. The latter proved the most effective.

Driving off excess layers

Heating the substrate to between 170 and 190°C was found to drive off the physically absorbed second layer of organic leaving a monolayer. Heating also broke up the adsorbed dimers. For temperatures less than 170°C, e.g. 150°C, a very thick wax like build up occurs. The resistance of the resulting junction has a resistance greater than 100 meg ohms. This large resistance indicates a massive build up of organic. The measured capacitance of such a junction is approximately 100 pf which indicates an insulator thickness of greater than 5000 $\overset{o}{A}$. If the substrate temperature is much above 190°C, e.g. 210°C, then a junction resistance of approximately 0.08 ohms results. No capacitance null is possible with these junctions. These data indicate a short circuit across the junction, i.e. no insulator.

With the substrate temperature held between 170-190°C, junctions of resistance between 1 to 10 ohms can be formed. This gives indirect evidence that monolayers of the organic have formed.

Organic Vapor

To create the organic vapor, the organic powder is heated in a quartz crucible. The temperature to which the organic is heated is not measured directly but the current which heats the crucible provides an indirect measure. The organic powder is a dimer, i.e. two monomers attached at their reactive ends. To form the monolayer, the dimer must be broken down with heat into the two monomers. Therefore, the organic must be sufficiently hot to cause the dimer breakdown. However, if the temperature becomes too hot then the organic splatters out of the crucible. A very narrow range of heating currents has been found suitable for proper film deposition. Below 27 amperes only short circuit junctions are formed. This indicates that dimer breakdown is not occurring. Above 31 amperes, spattering is a serious problem. We decided on 29 amperes.

Josephson junction procedure

The procedure found to best produce monolayer barriers is as follows:

1. 1" x 1" thermal glass is cleaned and placed in a substrate holder,

2. The vacuum system is pumped to below 2×10^{-5} Torr - this takes 10-15 minutes.

3. A lead strip is vacuum deposited on the glass substrate,

4. The substrate with Pb strip is then heated to approximate 180°C for 1.5 minutes,

5. The substrate is exposed to organic vapor (stearoyl peroxide) for 20 seconds,

6. The substrate is held at 180°C for an additional 1.5 minutes,

7. A cross strip of aluminum is vapor deposited on the organic-lead,

8. The junction is allowed to cool and self anneal for 1-5 hours in the vacuum.

III.   Increasing T_c with an organic layer

Brief summary

A number of surface enhancement investigations which employ the adsorption of thin layers of gases have been reported in the literature. As a part of our organic monolayer studies, we observed the effects of the organic layer on the T_c of our metal films. This part of the research program was not extensively pursued but some interesting results were observed which indicate that the T_c of Al was increased approximately 0.4°K.

Concept of surface enhancement of T_c

The principle behind surface enhanced T_c is one of increasing the net attractive interaction between electrons. There are several theoretical models to explain or predict enhancement. One such model envisions the adsorbing molecule as charging or discharging the surface via electron transfer. This seems to explain the T_c enhancements and depressions caused by the organic molecules adsorbed on vanadium reported by Hoffman et al.[3] This model does not fit the enhancement they observed after oxidation of the vanadium but this model does fit the oxidation and plate changing of Al observed by Glover[4] and Ruhl.[5,6]

Thin layers of Ge on Tl and Sn have also been observed[7] to change T_c. While the sign of the change fits the above charge transfer model, the magnitude to the required change transfer is unrealistically large.

However, S, Se and Cl compounds deposited on Tl and Sn yield results consistent with this model. [8]

The shift in T_c of Al, Sn, Tl and Bi due to the adsorption of the noble gases, Ar and Ne, has been explained [9] in terms of a modification of the phonon spectrum.

Ginzburg [10-12] and more recently Bardeen [13] have proposed an exciton-phonon interaction to increase the net attraction of the electron. In this model a suitable dielectric is either deposited on the metal or layers of metal and dielectric are formed or a thin metal is deposited on the dielectric. In all cases, the dielectric serves the purpose of providing the excitons. While there is no direct experimental evidence to support this model, some of the experimental results possibly can be explained by the exciton model.

In ending this section, it should be mentioned that several other mechanisms influence the T_c of thin superconductors. These are film density, disorder, crystallite size and mechanical strain. All of these mechanisms must be considered in interpreting experimental results.

Observed increase in T_c
_____

Increased T_c of Al was indirectly observed in the tunneling character-istics of Pb-Organic-Al junctions. The junctions were formed by the process outlined in section II. The V-I characteristics of a junction are shown in Fig. 1. Josephson tunneling is observed at $T \approx 1.3°K$. This is $0.13°K$ above the transition temperature of Al. Small bumps in the V-I curves are observed at $1.56°K$.

These curves show that the Al film is definitely superconducting. But why is not known. In the first place, the organic was deposited on the Pb film and is assumed to be bonded to this layer in such a manner or to extract electrons from the Pb. The Al film is deposited over this organic and is bonded via van der Waal forces and probably some oxidation bonding force, although this should not be strong. It should also be noted that this enhancement disappeared after storing the junction in room air for several days. During this time the junction resistance increased from about 1.3 to 3.0 . The cause of this increase in junction resistance is not known but it is assumed to be either an increase in the tunneling barrier thickness or the barrier height. For thin barriers, such as those used here, the tunneling resistance is approximately proportional to barrier thickness. This would imply that the barrier would double in thickness for a resistance change from 1.3 to 3.0. Thus it seems more reasonable to conclude that changes in the barrier height (which exponentially changes the resistance) is the cause of the junction aging. One might also conclude that the barrier change is due to a surface reaction at the organic-Al interface. This surface reaction may then be cause of the disappearance of the enhanced T_c.

IV. Analysis of Josephson Junctions and Interferometers

Brief Summary

A numerical technique was developed to solve the Josephson equations subject to the proper boundary conditions and geometrical configuration. Computations on a wide variety of junctions and interferometers have provided
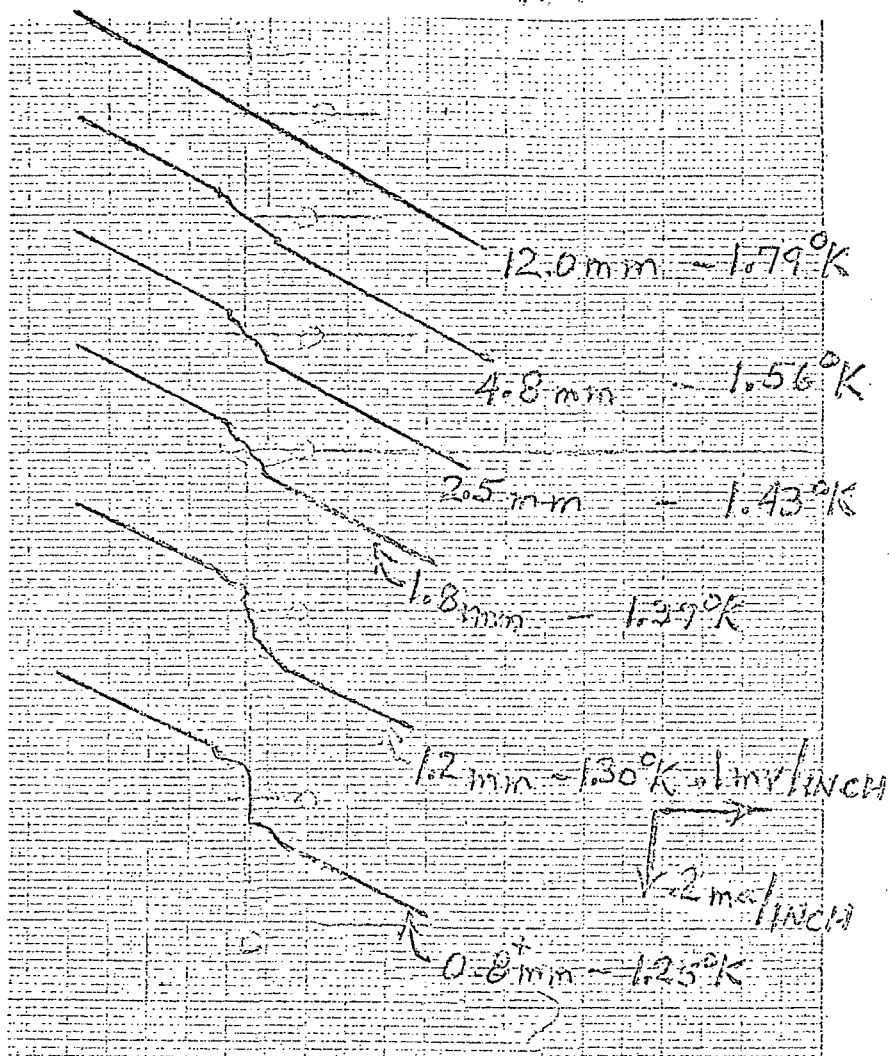
Figure 1. Current-voltage trace of Sample SP-11
at 1.79 to 1.25°K. Expanded scales.

considerable insight into the functioning of these devices. In addition,
the computer technique yields quantative data for the design of high
sensitivity magnetometers. This includes "exact" diffraction and inter-
ference patterns, as a function of the number of junctions, different size
junctions and loops, and mismatch of the junctions and loops. The many
details of these calculations are given in the five journal papers which
resulted from this work.

With the above work, it is now possible to design high sensitivity
magnetometers and determine their sensitivity to variations in fabrication
parameters, such as junction and loop mismatch. Thin film magnetometers
with a sensitivity of at least 10^{-9} Gauss has been shown to be possible.

Basic Equations

First, the equations describing a Josephson junction will be presented.
These will be used to formulate the equations for a Josephson junction
interferometer. Approximate and exact equations will be presented to
give an overall view of the theoretical work to date on Josephson junction
interferometers.

Josephson predicted that the current density, $J(x,y)$, through a thin
superconducting junction would be of the form

$$J(x,y) = J_1 \sin\phi(x,y) \tag{1}$$

where J_1 is the maximum current density and $\phi(x,y)$ is the pair phase across
the junction.

The equation

$$\Delta\phi(x,y) = \frac{2ed}{nc} \ H \times n \tag{2}$$

relates the gradient of the pair phase to the local magnetic field. d is
the barrier thickness plus twice the London penetration depth. H, the local

magnetic field, is composed of the applied magnetic field plus the magnetic field due to the current in the superconductors.

If one neglects the magnetic field due to the current, the total current through the junction as a function of the applied magnetic field has the following closed form solution.

$$I = \frac{I_o \sin(\pi \phi_J / \phi_o)}{\pi \phi_J / \phi_o} \, \phi \sin \, (o) \qquad . \tag{3}$$

I_o is the critical current density, J_1, times the area of the junction, LW. ϕ_J is the applied flux, HedL, and ϕ_o is the magnetic flux quantum nc/2e. $\phi(o)$, the phase in the middle of the junction, is set equal to $\pi/2$, consistent with maximizing the current through the junction.

The maximum current through the junction as a function of applied magnetic field is more complex if one does not neglect the self-induced magnet fields. To find the current Maxwell's equation

$$\Delta \times \vec{H} = \frac{4\pi}{c} \, J(x,y) \tag{4}$$

must be added to the set of equations describing the junction. Combining Eqns. 1, 2 and 4 one obtains

$$\frac{\partial^2 \phi}{\partial x^2} + \frac{\partial^2 \phi}{\partial y^2} = \frac{1}{\lambda_J^2} \sin\phi(x,y) \tag{5}$$

where λ_J, the Josephson penetration depth, is equal to $(nc^2/8\pi e d J_1)$. A decision must now be made as to the geometry of the junction to be solved. Eqn. 5 has only been solved for the linear and asymmetrical junction. The reason being that for these two geometries current only flows in the y direction, which is the same direction as the applied magnetic field. Thus Eqn. 5 simplifies to the ordinary differential equation.

$$\frac{d^2 \phi}{dy^2} = \frac{1}{\lambda_J^2} \sin\phi(y) \qquad . \tag{6}$$

Also, the total current will now be proportional to the width of the junction which is in the x direction. These simplifications are not valid for the crossed junction.

The boundary conditions for the linear Josephson junction are found using Amperes Law and Eqn. 2.

$$\frac{d\phi}{dy}\bigg|_{y=L} + \frac{d\phi}{dy}\bigg|_{y=0} = \frac{4ed}{\hbar c} H_e \qquad (7)$$

$$\frac{d\phi}{dy}\bigg|_{y=L} - \frac{d\phi}{dy}\bigg|_{y=0} = 8\pi edI/\hbar c^2 w \qquad (8)$$

L is the junction length.

Owen and Scalapino[19] solved graphically Eqn. 6 subject to Eqns. 7 and 8. Their principal result was that the total current was proportional to length for junction of length less than $2\lambda_J$. For junctions of length greater than $6\lambda_J$ the total junction current saturated and stayed constant at I = $4\lambda_J wJ$. This implied that the Fraunhofer diffraction pattern was a good approximation for junctions of length less than $2\lambda_J$. Owen and Scalapino[14] also predicted a linear dependence of current on magnetic field for junctions of length L = $10\lambda_J$.

The boundary conditions for an asymmetrical junction[15] are

$$\frac{d\phi}{dy}\bigg|_{y=L} = \frac{2ed}{\hbar c} H_e \qquad (9)$$

$$\frac{d\phi}{dy}\bigg|_{y=L} - \frac{d\phi}{dy}\bigg|_{y=0} = \frac{8ed\pi I}{\hbar c^2 w} \qquad (10)$$

Boundary Eqns. 7, 8, 9 and 10 are important in the analysis of interferometers.

The first analysis of a two junction interferometer was based on summing the currents through two Josephson junctions, one placed at $L=0$ and the other at $L=L_1$. The junctions were considered to be equal

$$I = \frac{I_o \, \sin(\pi\Phi_J/\Phi_o)}{\pi \, \Phi_J/\Phi_o} \, (\sin\phi(o) + \sin\phi(L_1)) \qquad (11)$$

Again by neglecting the self-currents, $\phi(L_1)$ can be solved in terms of $\phi(o)$ and H_e by solving Eqn. 2 directly.

$$\phi(L_1) = \phi(o) + \frac{2eA}{\hbar c} H_e \qquad (12)$$

Here, A is the interference loop area. Eqn. 11 then simplifies to

$$I = \frac{2I_o \, \sin(\pi\Phi_J/\Phi_o)}{\pi \, \Phi_J/\Phi_o} \, \cos(\frac{eA}{\hbar c} H_e) \qquad (13)$$

by assuming $\phi(o)$ adjusts such that $\phi(o) + \frac{eA}{\hbar c} H_e = \pi/2$ i.e. current is maximized. In Eqn. 13 the sine term is the diffraction term and the cosine term is the interference term.

DeWaele and DeBruyn Ouboter[16,17] included in their analysis the effects of self-induced magnetic fields in the interference loop. To accomplish this, the inductance, z, of the loop times the loop current is added to Eqn. 12 to obtain

$$\phi(L_1) = \phi(o) + \frac{2e}{\hbar c} AH_e + \frac{I_o z}{2} (\sin\phi(o) - \sin\phi(L_1)) \qquad . \quad (14)$$

Eqn. 14 is then solved simultaneously with Eqn. 11 to obtain the interference

pattern. All analyses to date which include the self-induced flux have set the diffraction term equal to one.[18,16,19]

The major result obtained from including the self flux in the interference loop was that the minimums in the interference pattern do not go to zero current. This result is in agreement with the experimental work.

Clarke and Patterson[18] observed that one specific geometry (the asymmetrical current feed interferometer) produced an interference pattern with increased magnetic field sensitivity. They mathematically modeled this case by setting $\sin\phi(o) = 0$ in Eqn. 14. Their theoretical results qualitatively matched their experimental work.

DeWaele and DeBruyn Ouboter[16,17] solved the magnetic field behavior of multiple point contact interferometers. They neglected junction effects, self-currents and diffraction effects and derived

$$I = I_o \frac{\sin\left\{N\left[\dfrac{2eAH_e}{\hbar c}\right]\right\}}{\sin\left[\dfrac{2eAH_e}{\hbar c}\right]} \tag{15}$$

In Eqn. 15 N is the number of junctions. Their experimental results[16,17] did not closely follow Eqn. 15, for $N = 2,3,4,5$.

At Colorado State University we have developed an analysis technique for theoretically predicting the magnetic field characteristics of multiple Josephson junction interferometers. The Josephson penetration depth effects geometry, and junction-interference loop coupling is included in the analysis.

The mathematical formulation follows the work of Owen and Scalapino[14] who solved the one junction case. Their results have been experimentally verified in detail.[20,21] For a symmetrical interferometer composed of N

linear Josephson junctions, the boundary conditions are

$$\frac{d\phi}{dy}\bigg|_{y=L_{2N-1}} + \frac{d\phi}{dy}\bigg|_{y=0} = \frac{4ed}{\hbar c} H_e \tag{16}$$

$$\frac{d\phi}{dy}\bigg|_{y=L_{2N-1}} - \frac{d\phi}{dy}\bigg|_{y=0} = 8\pi ed I/\hbar c^2 w \quad . \tag{17}$$

The coupling between junctions and interference loops is obtained from observing continuity of magnetic field at the junction-interference loop boundaries. Then Eqn. 2 can be solved directly to give the coupling between the phase and the first derivative of phase at the junction-interference loop boundaries.

$$\phi_2 = \phi_1 + \frac{d_2}{d_1} \frac{d\phi}{dy} (L_1)(L_2 - L_1)$$

$$\phi_4 = \phi_3 + \frac{d_2}{d_1} \frac{d\phi}{dy} (L_3)(L_4 - L_3) \tag{18}$$

$$\phi_{2N-2} = \phi_{2N-3} + \frac{d_2}{d_1} \frac{d\phi(2N-3)}{dy} \quad L_{2N-2} - L_{2N-3}$$

The L_N's refer to the edges of the various Josephson junctions (see Fig. 1). In Eqn. 18 N is the number of junctions comprising the interferometer. The self-induced flux in the interference loops is therefore incorporated into the set of equations by observing continuity of magnetic field at the interference loop-junction boundaries, i.e.

$$\left.\frac{d\phi}{dy}\right|_{y=L_1} = \left.\frac{d\phi}{dy}\right|_{y=L_2}$$

$$\cdot$$

$$\left.\frac{d\phi}{dy}\right|_{y=L_3} = \left.\frac{d\phi}{dy}\right|_{y=L_4} \qquad (19)$$

$$\cdot$$
$$\cdot$$
$$\cdot$$

$$\left.\frac{d\phi}{dy}\right|_{y=L_{2N-2}} = \left.\frac{d\phi}{dy}\right|_{y=L_{2N-3}}$$

Eqns. 6, 16, 17, 18 and 19 completely describe the critical current-magnetic field behavior of the interferometer. The equations can be solved numerically to determine the interference and diffraction patterns of symmetrical current feed multiple junction interferometers.

The asymmetrical current feed interferometer has a different set of boundary conductions than the symmetrical current feed interferometer. They are

$$\left.\frac{d\phi}{dy}\right|_{y=o} = \frac{2ed_1}{\hbar c}\,[H_e - 4\pi I/cw] \qquad (20)$$

and

$$\left.\frac{d\phi}{dy}\right|_{y=L_{2N-1}} = \frac{2ed_1\,H_e}{\hbar c} \qquad (21)$$

Therefore Eqns. 6, 18, 19, 20 and 21 describe the operation of the asymmetrical current feed interferometer.

Numerical Method

The numerical solution method is based on transforming the boundary value problem to an initial value problem. The input to the numerical solution method contains the estimated value of current, I, the applied magnetic field H_e and the detailed dimensions of the interferometer. For a given applied magnetic field and current, the first derivatives of the phase at $y = 0$ and $y = L_5$ are computed from Eqns. (5) and (6) or (7) and (8). The value of the phase at $y = 0$ is iterated between zero and 2π until the first derivative of the phase at $y = L_5$, obtained from the solution of Eqn. (4)[22], equals that obtained from the solution of Eqns. (5) and (6) or (7) and (8). If no solution is found the selected current is greater than the critical current and a lower value of current is then selected. This process continues until a solution to the equations is found. The demarcation between finding a solution and not finding a solution to the equations is the critical current. The error in phase depends on the increment size, the junction size and interference loop area. A computer program flow diagram for a three junction interferometer is shown in Fig. 2. For each junction and interference loop added to the interference grating a block similar to the dashed block in Fig. 2 must be added.

The computed results are presented in terms of the Josephson penetration depth, the length of the junctions and the area of the interference loops which is in contrast with previous authors[23-25] who present their interference patterns in terms of total current and inductance.
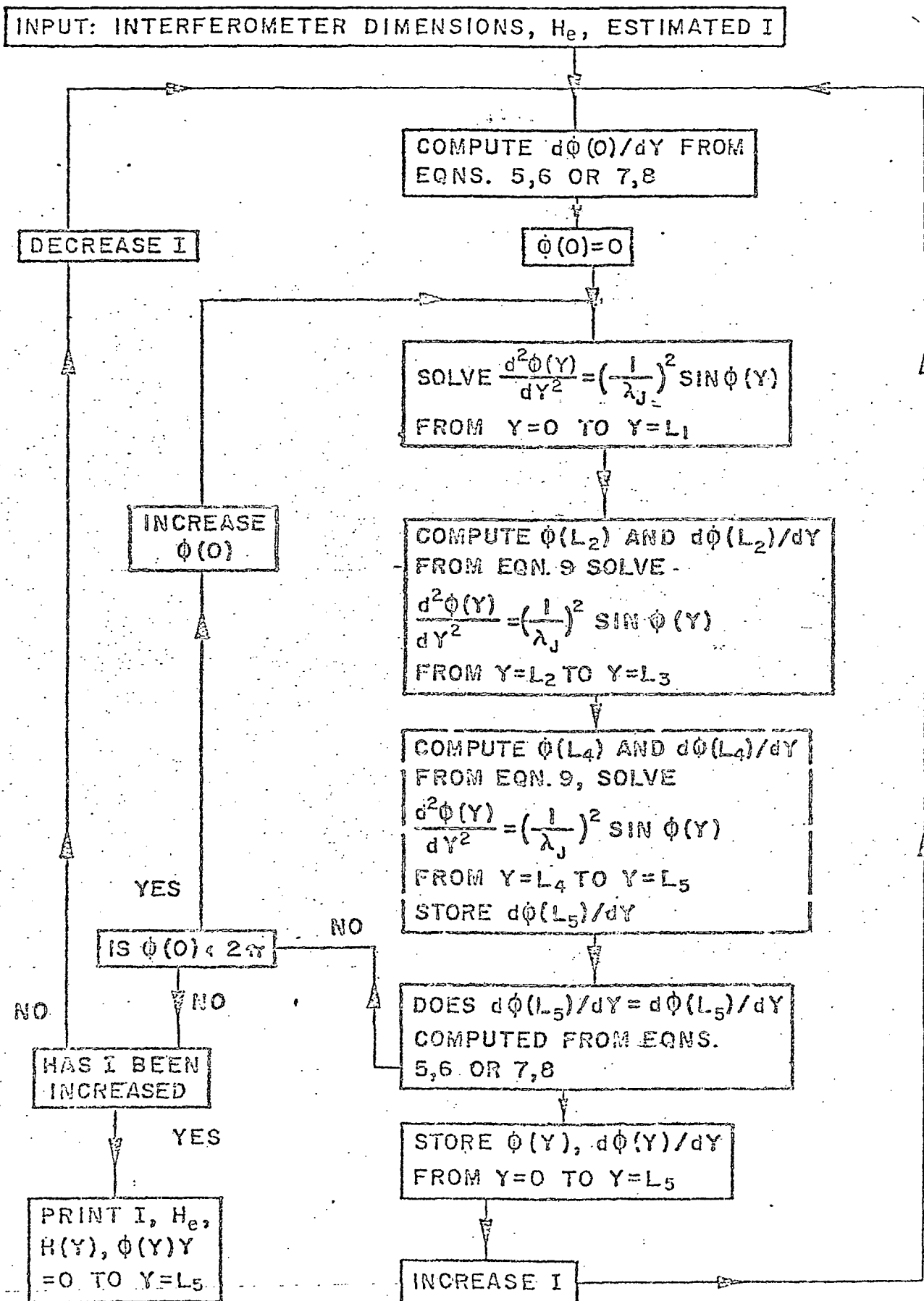
INPUT: INTERFEROMETER DIMENSIONS, H_e, ESTIMATED I

COMPUTE $d\dot\phi(0)/dY$ FROM EQNS. 5,6 OR 7,8

DECREASE I

$\dot\phi(0)=0$

SOLVE $\dfrac{d^2\phi(Y)}{dY^2}=\left(\dfrac{1}{\lambda_J}\right)^2 \mathrm{SIN}\,\phi(Y)$

FROM $Y=0$ TO $Y=L_1$

INCREASE $\phi(0)$

COMPUTE $\dot\phi(L_2)$ AND $d\dot\phi(L_2)/dY$ FROM EQN. 9 SOLVE

$\dfrac{d^2\phi(Y)}{dY^2}=\left(\dfrac{1}{\lambda_J}\right)^2 \mathrm{SIN}\,\phi(Y)$

FROM $Y=L_2$ TO $Y=L_3$

COMPUTE $\dot\phi(L_4)$ AND $d\dot\phi(L_4)/dY$ FROM EQN. 9, SOLVE

$\dfrac{d^2\phi(Y)}{dY^2}=\left(\dfrac{1}{\lambda_J}\right)^2 \mathrm{SIN}\,\phi(Y)$

FROM $Y=L_4$ TO $Y=L_5$

STORE $d\dot\phi(L_5)/dY$

YES

IS $\dot\phi(0) < 2\gamma$ NO

NO

DOES $d\dot\phi(L_5)/dY = d\dot\phi(L_5)/dY$ COMPUTED FROM EQNS. 5,6 OR 7,8

HAS I BEEN INCREASED

STORE $\phi(Y)$, $d\dot\phi(Y)/dY$ FROM $Y=0$ TO $Y=L_5$

YES

PRINT I, H_e, H(Y), $\phi(Y)Y$ $=0$ TO $Y=L_5$

INCREASE I

Figure 2
Flow diagram for computer program

Josephson Junctions

The result of our work on single junctions fall into two categories:

a) The variation of junction current with junction width and
perimeter.[26]

b) The boundary condition, diffraction patterns, and vortex
structure of asymmetrical and crossed junctions.[15]

The results of these investigations are discussed separately.

The critical current through a Josephson was reported in the literature

to be proportional to the perimeter of the junction. This was thought

true because of the current peaks at the edges of the length. However,

replotting the experimental data of Pritchard and Schroen[20] and plotting our

calculated value (fig. 3),[26] we were able to show that the critical current

was proportional to the width of the junction and not the perimeter.

We have examined the boundary conditions for the asymmetrical and cross

Josephson junctions.[15] A striking similarity appears between the diffraction

patterns of the two geometries.

The boundary conditions for the asymmetrical Josephson junction

are obtained by applying Amperes law at the boundaries. These are:

$$H(o) = H_e - 4\pi I/cW$$

$$H(L) = H_e \cdot$$

These imply that no current flows in the lower part of the bottom

superconductor nor in the upper part of the top superconductor.

The boundary conditions for the cross junction depend on

assumptions made about the current flow in the device. One possibility,

which we will call case I is that part of the current flows on each side

of the superconductor leads. The positive direction of $H(o,y)$, $H(W,Y)$,

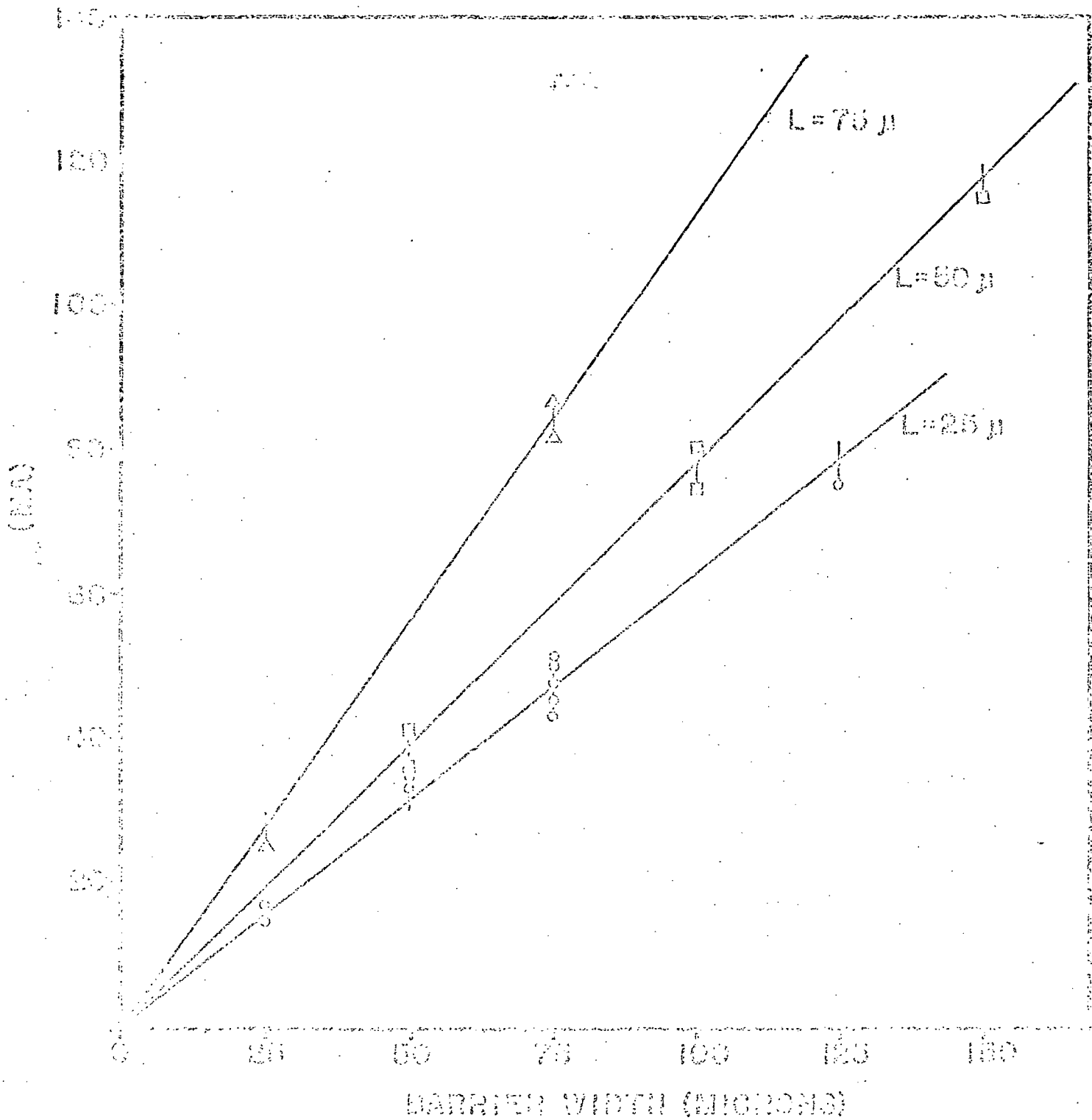$H(x,o)$ and $H(x,L)$ are assumed to be in the positive y and negative x

Figure 3.

Replotting of the data of Schroen and Pritchard.

directions. The boundary conditions are then

$$W(H_e + H_{i1} - H_x(x,o)) = 4\pi I/c \tag{22}$$

$$W(H_x(x,L) - H_e) = 0 \tag{23}$$

$$L(H_{i2} + H_y(\omega,y)) = 4\pi I/c \tag{24}$$

$$H_y(o,y) = 0 \tag{25}$$

$$L\,H(W,y) + WH(x,L) - L\,H(o,y) - WH(x,o) = 4\pi I/c. \tag{26}$$

H_{i1} is the magnetic field due to the current flowing on the underside of the superconductor at $y = 0$. H_{i2} is the magnetic field due to the current flowing on the top of the superconductor at $x = W$. The important point about these boundary conditions is that there are magnetic fields in the y direction in the junction. This implies that the current density is not uniform in the x direction. In addition there is no magnetic field applied in the y direction to cancel the self-field so the maximum critical current will be less than the theoretical maximum.

A different set of boundary conditions is also applicable to the cross geometry if one assumes a different current path in the junction. The current entering the junction in the positive y direction can set up an image current in the negative y direction in the upper superconductor. The current in the upper superconductor is then assumed to flow around the edge of the top superconductor at $y = 0$ and flow in the positive x direction on the top of the superconductor. The boundary conditions for this current flow called case II are:

$$W(H(x,L) - H_e)) = 0 \tag{27}$$

$$H(o,y) = 0 \tag{28}$$

$$L(H(W,y) + H_i)) = 4\pi I/c \tag{29}$$

$$W(H_e - H(x,o)) = 4\pi I/c \tag{30}$$

$$-WH(x,o) + L\,H(W,y) + WH(x,L) - L\,H(o,y) = 4\pi I/c. \tag{31}$$

H_i is the magnetic field in the negative y direction on top of the superconductor at $x = W$ and is equal to $4\pi I/cL$ from Eqs. 26-31. Equation 29 then states that $H(W,y)$ is zero and therefore these boundary conditions are identical to the asymmetrical junction boundary conditions.

With these boundary conditions the diffraction patterns can be computed. These are shown in Fig. 4 and Fig. 5 for $L = 2\lambda_s$ and $L = 6\lambda_J$.
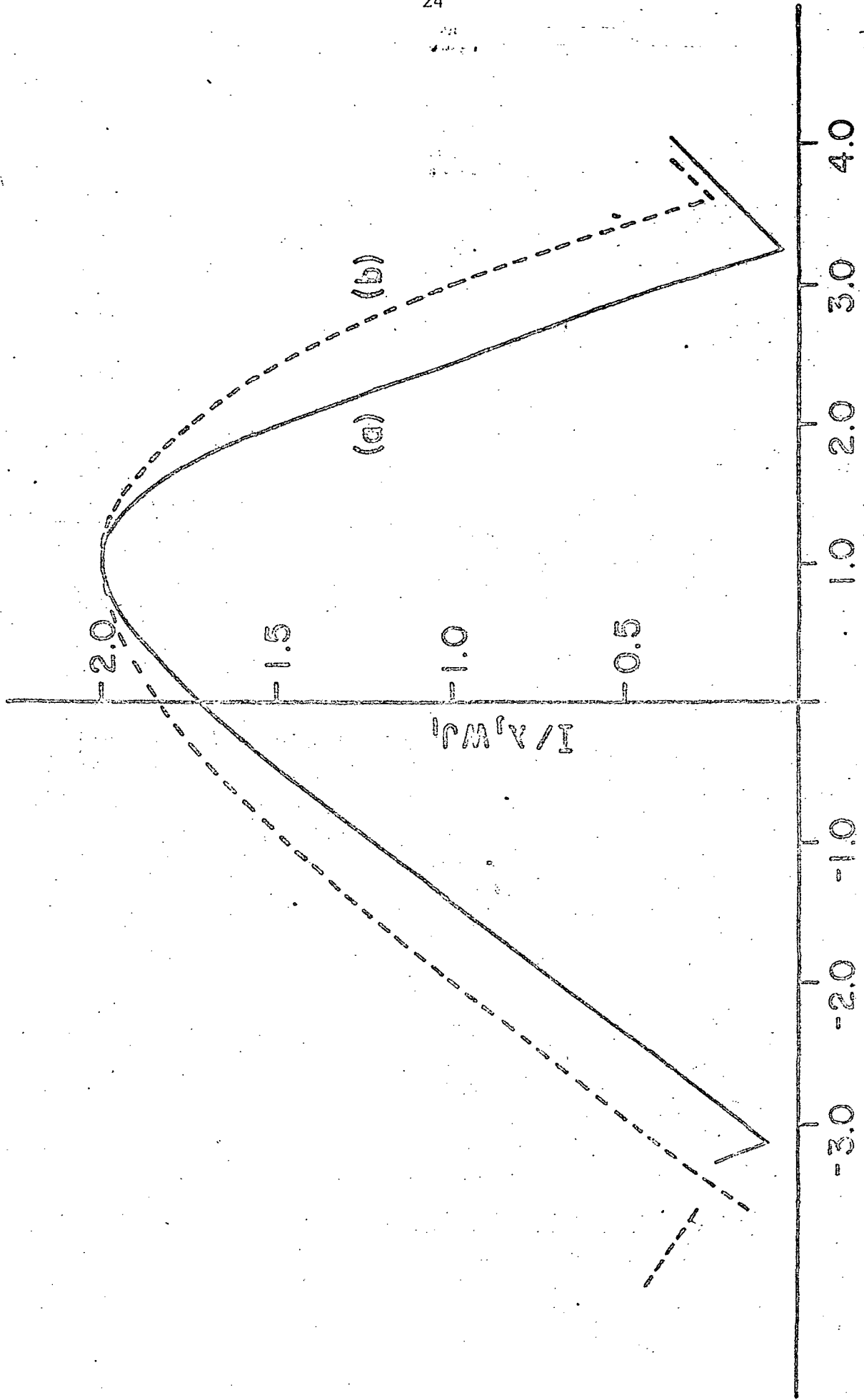
Diffraction patterns a) asymmetrical junction computed $L = 2\lambda_J$, and b) cross junction, experimental $L = 1.94\lambda_J$. Figure 4.
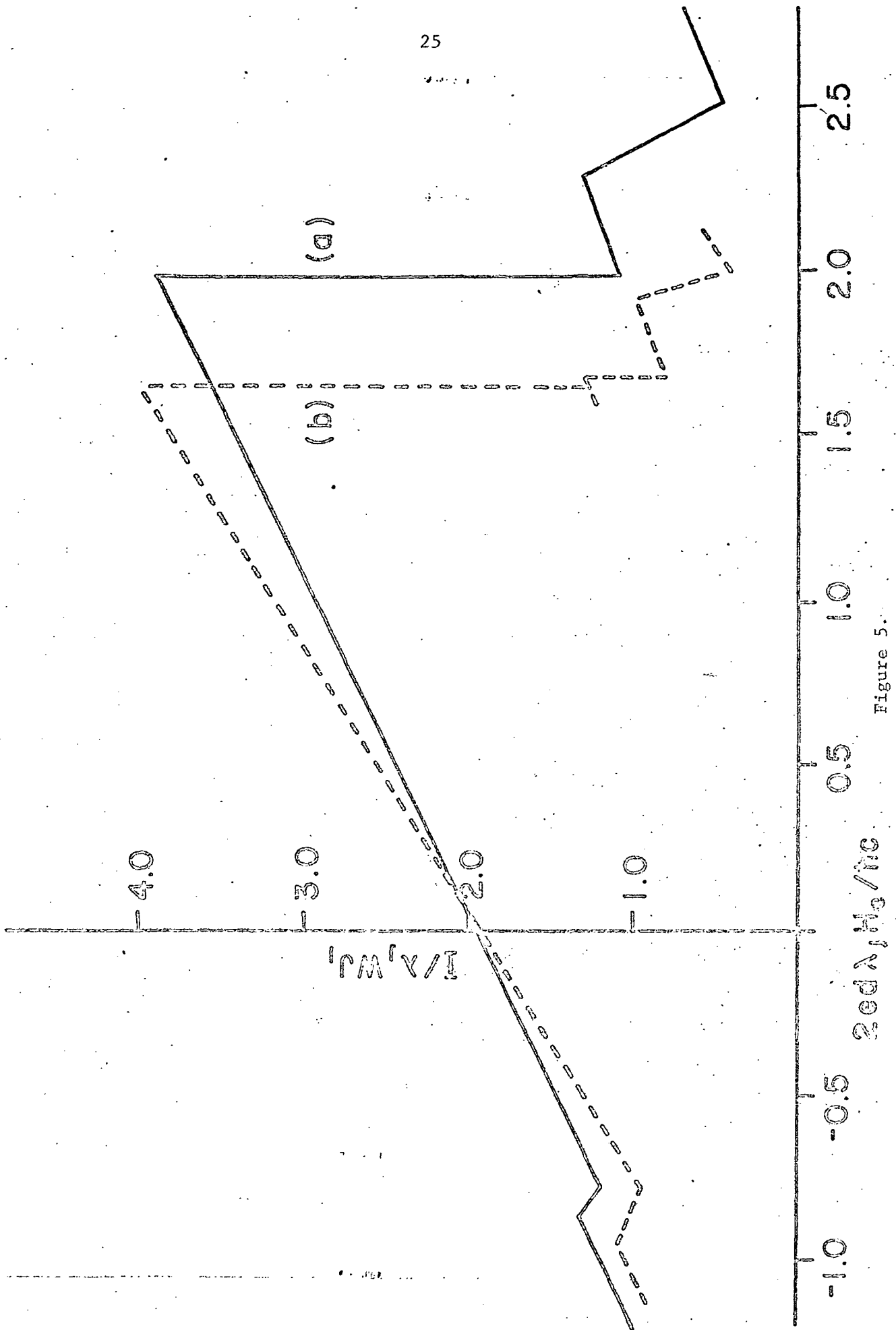
Figure 5. Diffraction patterns a) asymmetrical junction computed, $L = .6\lambda_J$ and b) cross junction, experimental, $L = 8.43\lambda_J$.

Josephson Interferometer
27-29

We have used the numerical method to generate and analyze multiple

junction interferometers (Fig. 6). The major results are summarized here.

The variation of the interference patterns with change in loop area for

three junction asymmetrical current feed interferometers are shown in Fig. 7.

These three curves exemplify the power of the numerical method to determine

details of the interference patterns and not just give a general outline of

the pattern features. What is also seen is the variation of pattern amplitude

and steepness of the slope of the main peak. The large amplitude change is

desirable since it provides a more easily detectable signal. The steeper

the slope the greater the sensitivity of the interferometer. For these

3 junction interferometers a large and small amplitude mode are observed.

This can be explained in terms of the phase and flux in the two interference

loops.

Typical interference patterns for 2, 3, 4, and 5 junction asymmetrical

current feed interferometers are shown in Fig. 8. Here the total loop area

and the junction length are held constant. Note, that the amplitude and

steepness of the major peak increases with the number of junction. This is

shown separately in Figs. 9 and 10. Junction length mismatch has been found

not to strongly effect the 2 junction patterns. The effects of junction

mismatch on the 3,4 and 5 junction interferometers have not been determined.

For the two junction interferometer, the variation of pattern amplitude

as a function of junction length is shown in Fig. 11. Here the loop area is

a parameter. The change in interference patterns with junction mismatch

for the 2 junctions interferometer is shown in Fig. 12.

Along with each computed point on the diffraction and interference

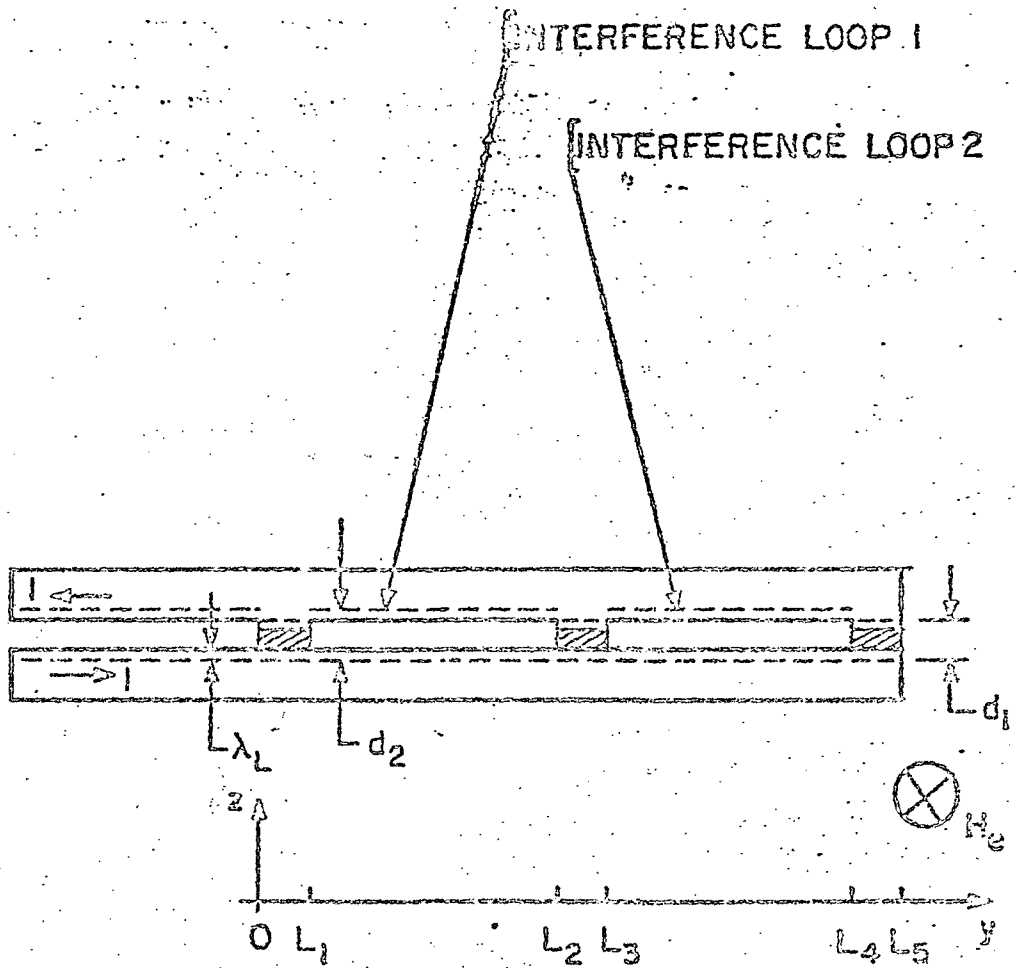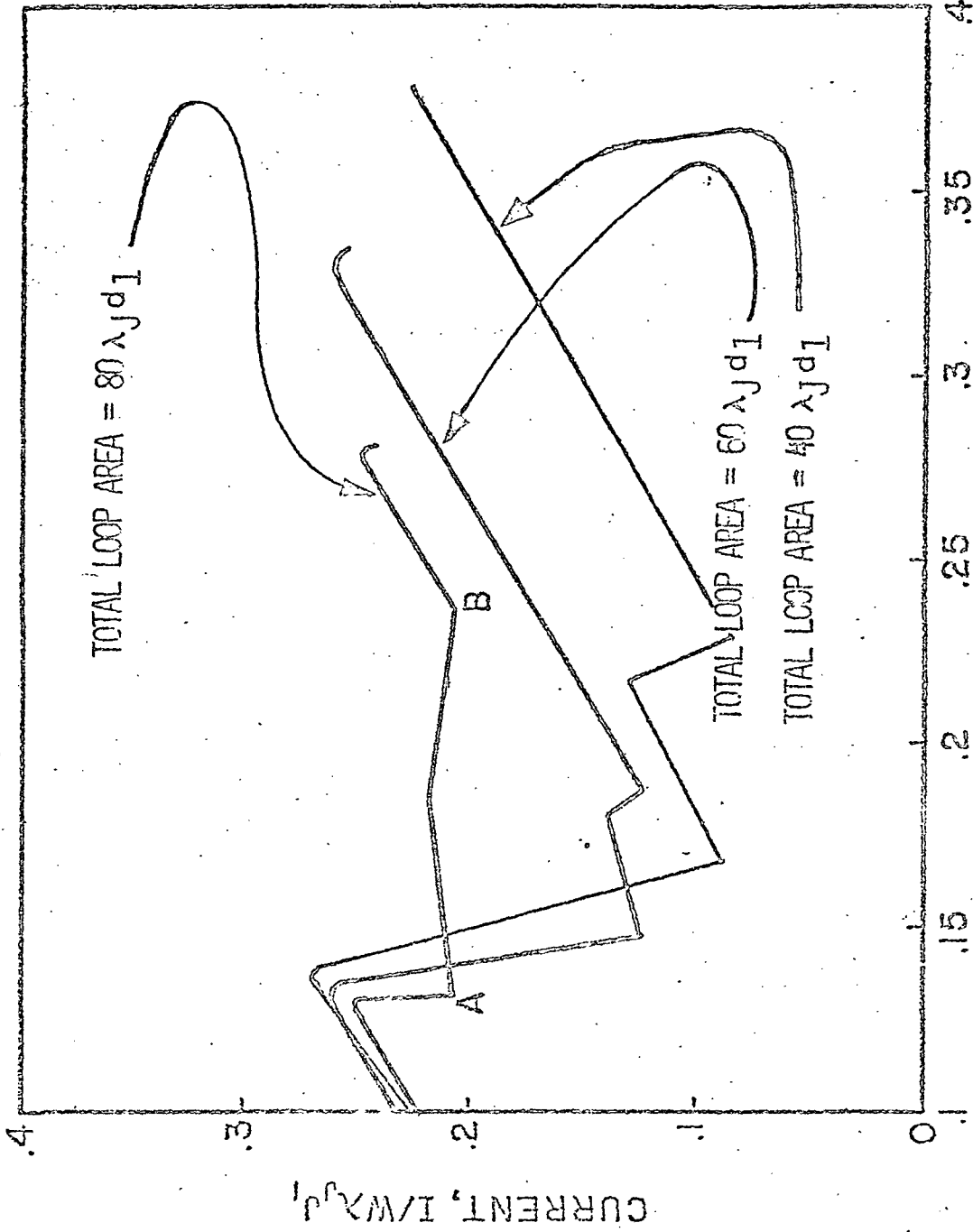pattern curves, one also computes the current and flux distribution for the

Figure 6. The geometry of a three junction asymmetrical current feed interferometer.

3. JUNCTION INTERFEROMETER
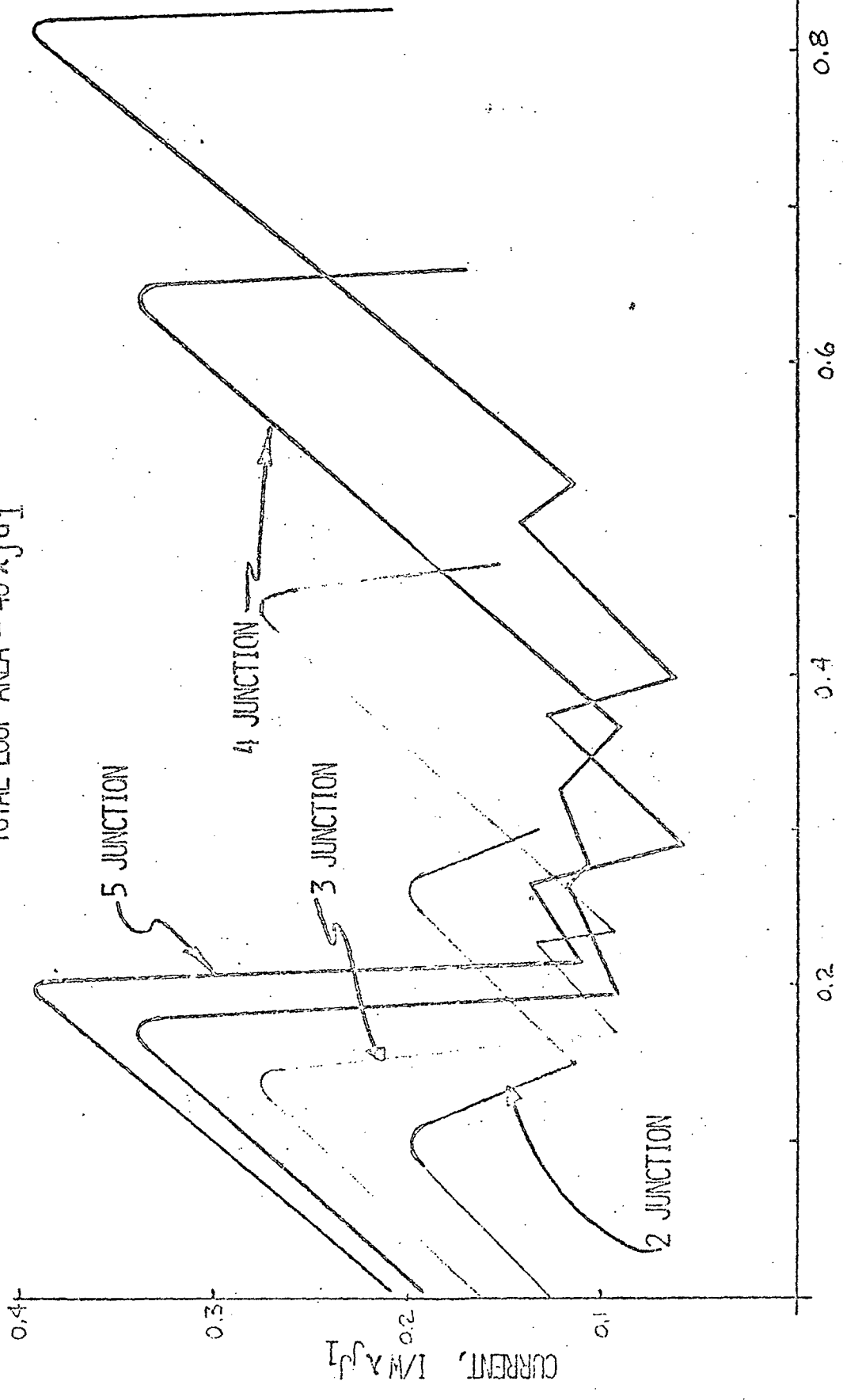
JUNCTION LENGTH = $0.1 \lambda_J$

TOTAL LOOP AREA = $80 \lambda_J d_1$

TOTAL LOOP AREA = $60 \lambda_J d_1$

TOTAL LOOP AREA = $40 \lambda_J d_1$

APPLIED MAGNETIC FIELD, $2 e d_1 \lambda_J H e / \hbar c$

CURRENT, $I / W \lambda_J J_1$

Figure 7. The interference pattern of a 3 junction interferometer for 3 values of loop area.

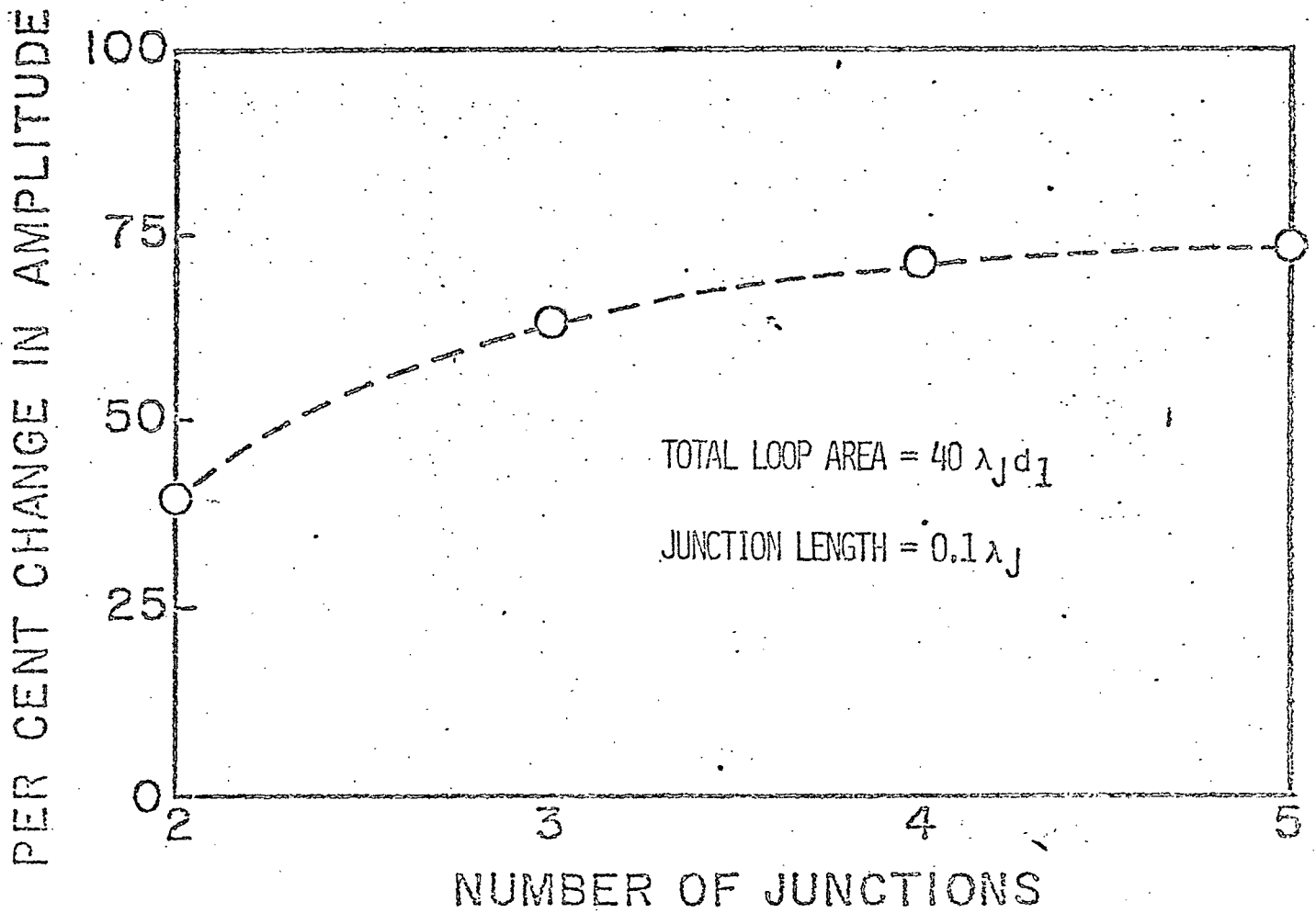Figure 8. Interference patterns of 2, 3, 4 and 5 junction asymmetrical current feed interferometers.

Figure 9. Percent change in interference amplitude with an increasing number of junctions for asymmetrical current feed interferometers.
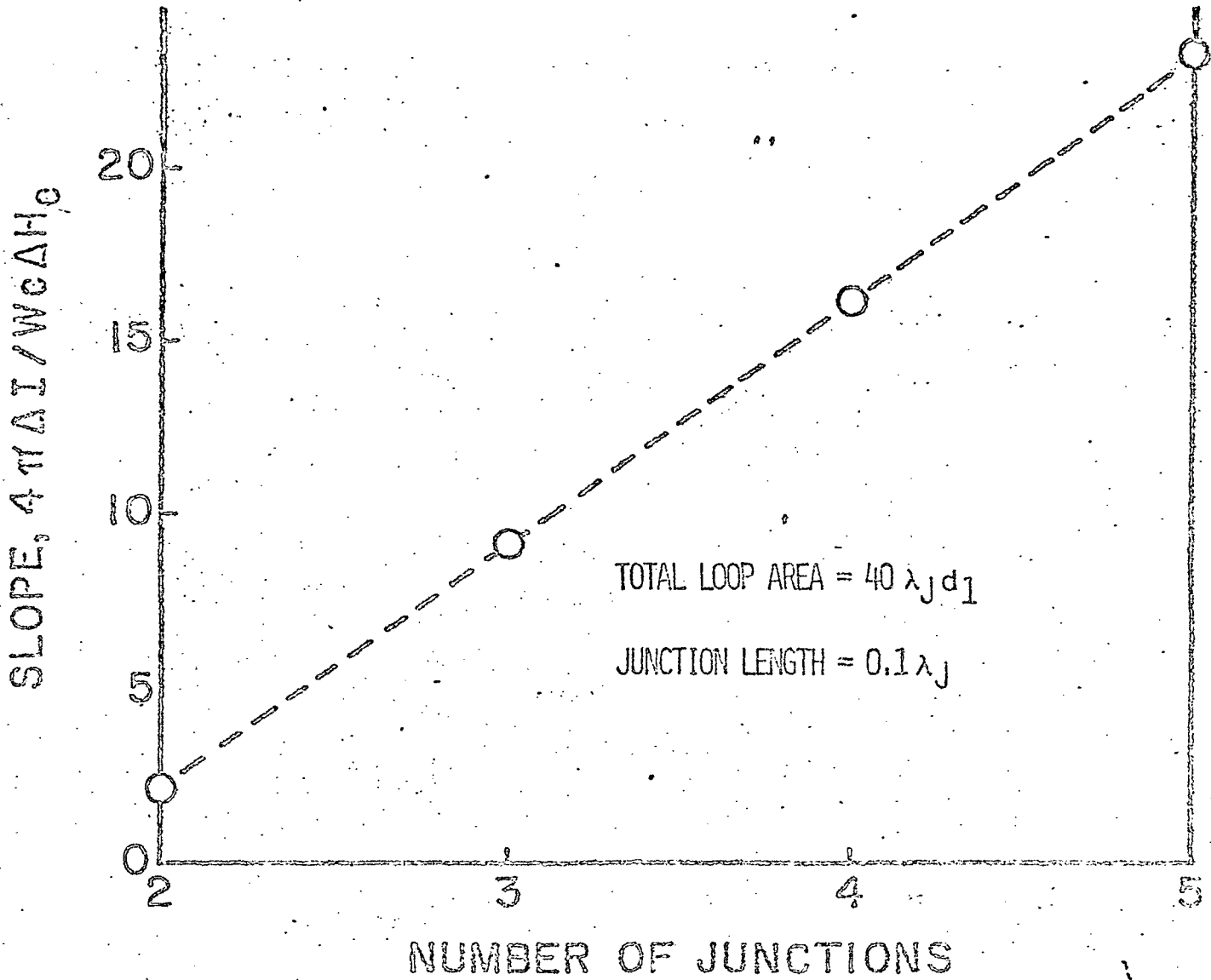
Figure 10. Maximum interference pattern slope as a function of the
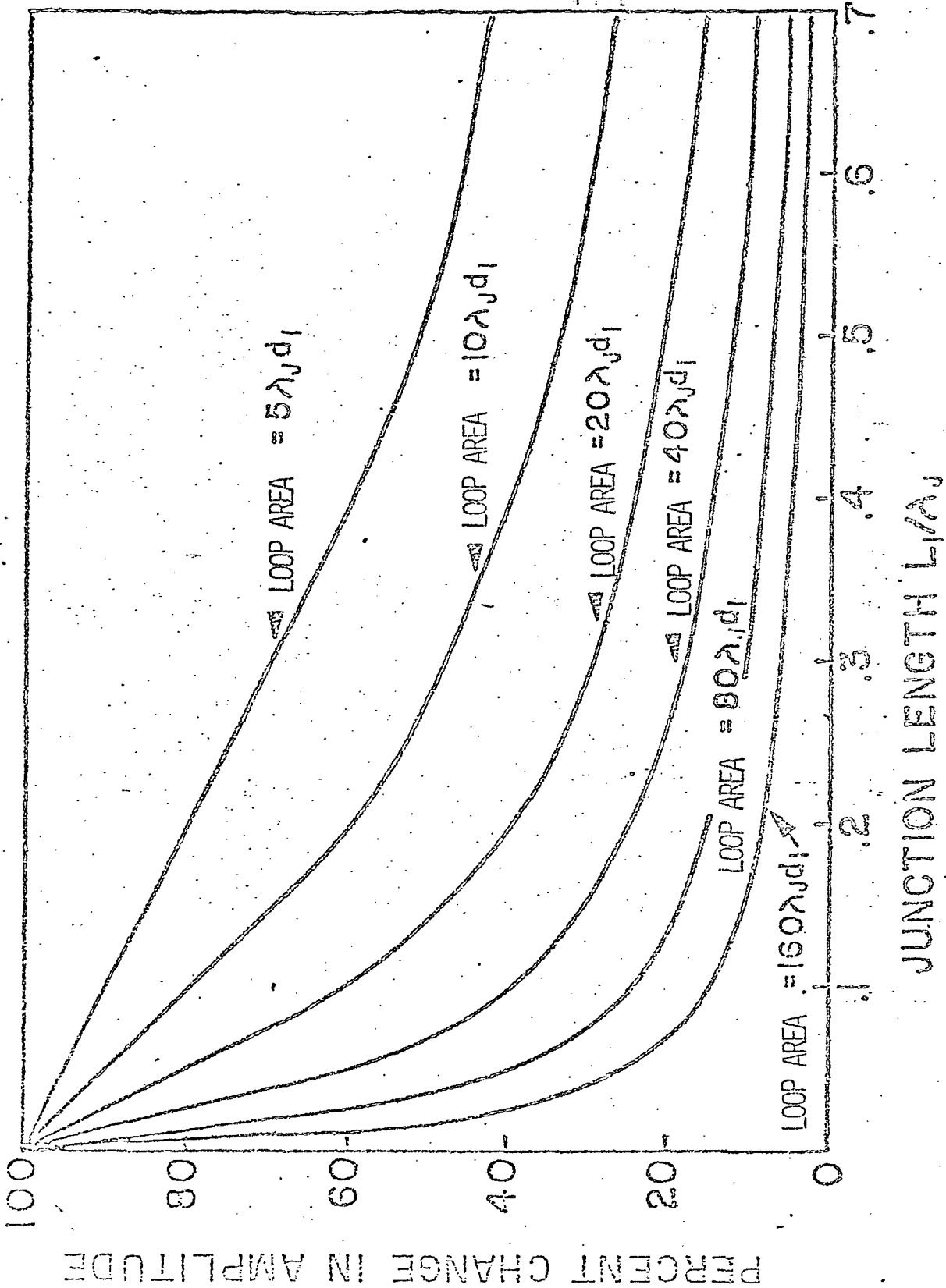number of junctions for asymmetrical current feed inter-
ferometers.

Figure 11. Percent change in interference pattern amplitude as a function of junction length for a 2 junction asymmetrical current feed interferometer.
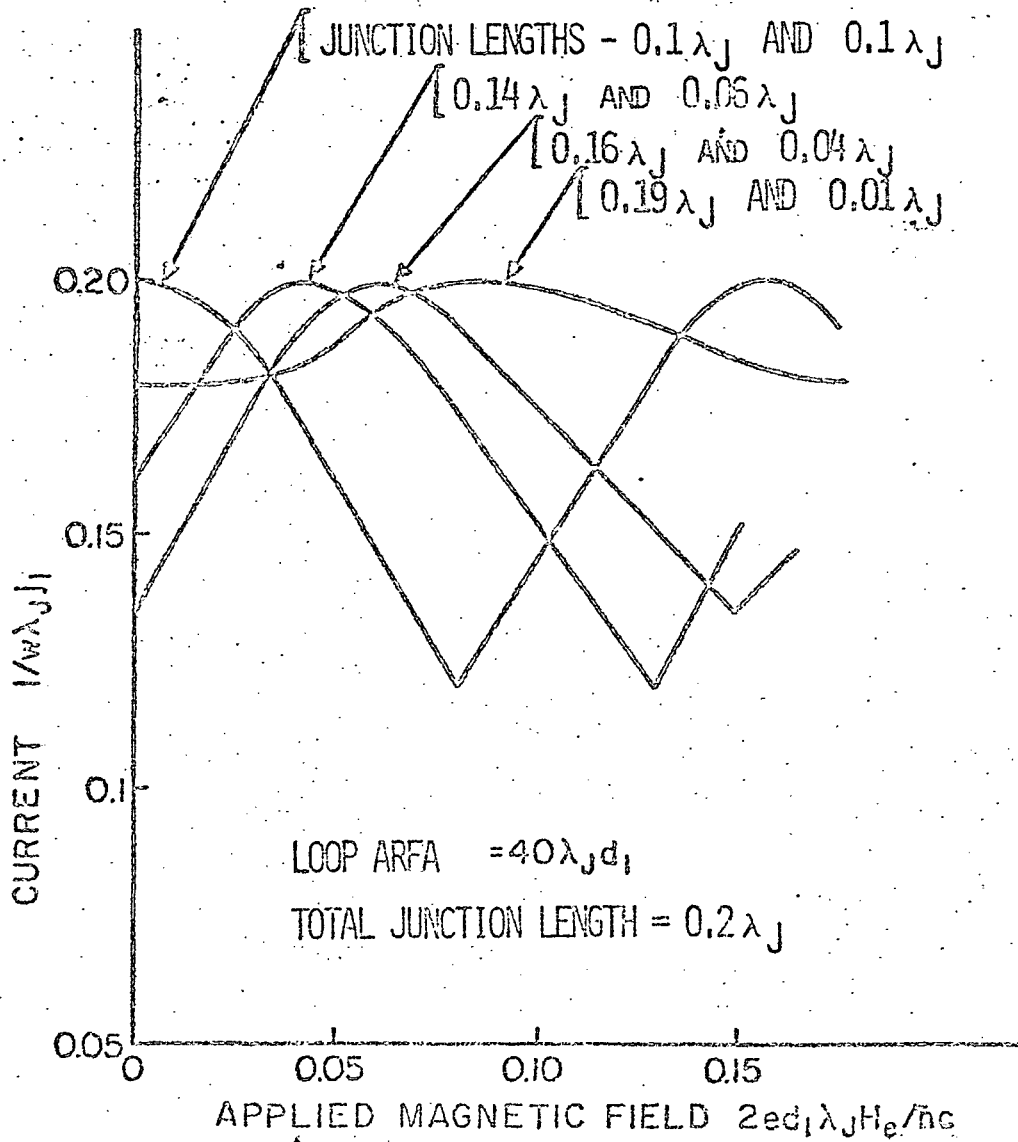
Figure 12.   Effect of unequal junction lengths on the

interference pattern of a 2 junction symmetrical

current feed interferometer.

entire interferometer. From all of this data, a better understanding of the interferometer is obtained along with a quantitative basis of designing and optimizing the interferometer.

References

1. J. C. Robertson and C. W. Wilmsen, "Extended Huckel Calculations of Relative Chemisorption Energies, J. Vac. Sci. and Tech. 8, 53 (1971).

2. J. C. Robertson and C. W. Wilmsen, "Preferential Orientation of CO Adsorption on Ni as Determined by Extended Huckel Calculations, J. Vac. Sci. and Tech., 9, 901 (1972).

3. B. M. Hoffman, F. R. Gamble, H. M. McConnell, J. Am. Chemical Society 89, 27 (1967).

4. R. E. Glover, III and M. D. Sherrill, "Changes in Superconducting Critical Temperature Produced by Electrostatic Changing," Phys. Rev. Letters 5, 248 (1960).

5. R. E. Glover, III and W. Ruhl, 10th Intl. Conf. on Low Temp. Phys., Moscow (1966).

6. W. Ruhl, "Zur Anderung der Ubergangstemperatur Verschiedener Supraleiter durch Elektronenentzug," Zeitshrift fur Physik 196, 464 (1966).

7. D. G. Naugle, "The Effect of Very Thin Ge Coating on the Superconducting Transistion of Thin Sn and Tl Films," Phys. Letters 25A, 688 (1967).

8. P. Hilsch and D. G. Naugle, "The Influence of Dielectric Films on the Superconductivity of Thin Sn and Tl Films," Zeitschrift fur Physik 201, 1 (1967).

9. D. G. Naugle, J. W. Balser and R. E. Allen, "Evidence for a Surface-Phonon Contribution to Thin-Film Superconductivity Depression of T_c by Noble-Gas Overlayers," Phys. Rev. B 7, 3028 (1973).

10. V. L. Ginzburg, "On Surface Superconductivity," Phys. Letters 13, 101 (1964).

11. V. L. Ginzburg, "Concerning Surface Superconductivity," J. Exptl. Theoret. Phys. (U.S.S.R.) 47, 2318 (1964).

12. V. L. Ginzburg, "The Problem of High Temperature Superconductivity," Contemp. Phys. 9, 355 (1968).

13. David Allinder, James Bray and John Bardeen, "Model for an Exciton Mechanism of Superconductivity," Phys. Rev. B 7, 1020 (1973).

14. C. S. Owen and D. J. Scalapino, "Vortex Structure and Critical Currents in Josephson Junctions," Phys. Rev. 164, 538 (1967).

15. D. L. Stuehm and C. W. Wilmsen, "Diffraction Patterns and Vortex Structure of Asymmetrical and Cross Josephson Junctions," J. Appl. Phys. to be published.

16. A. Th. A. M. DeWaele and R. DeBruyn Ouboter, "Quantum Interference Phenomena in Point Contacts Between Two Superconductors," Physica 41, 255 (1969).

17. A. Th. A. M. DeWaele and R. DeBruyn Ouboter, *Progress in Low Temperature Physics*, edited by C. J. Gorter, North-Holland Publ. Co., Amsterdam.

18. J. Clarke and J. L. Patterson, "Josephson Junction Amplifier," Appl. Phys. Letters 19, 451 (1971).

19. T. A. Fulton, L. N. Dunkleberger and R. C. Dynes, "Quantum Interference Properties of Double Josephson Junctions," Phys. Rev. 6, 855 (1972).

20. Walter Schroen and J. Paul Pritchard, Jr., "Maximum Tunneling Super-currents through Josephson Barriers," J. Appl. Phys. 40, 2118 (1969).

21. Klaus Schwidtal, "Type-I and Type-II Superconductivity in Wide Josephson Junctions," Phys. Rev. B 2, 2526 (1970).

22. J. M. Rowell, "Magnetic Field Dependence of the Josephson Tunnel Current," Phys. Rev. Letters 11, 200 (1963).

23. J. Clarke, "Electronics with Superconducting Junctions," Phys. Today 24, 30 (1971).

24. O. Doyle, "Josephson Junctions Leave the Lab...," Electronics 44, 38 (1971).

25. J. E. Zimmerman, Paul Thiene and J. T. Harding, "Design and Operation of Stable rf-Biased Superconducting Point-Contact Quantum Devices, and a Note on the Properties of Perfectly Clean Metal Contacts," J. Appl. Phys. 41, 1572 (1970).

26. D. L. Stuehm and C. W. Wilmsen, "Geometrical Dependence of the Maximum DC Josephson Current," J. Appl. Phys. 42, 869 (1971).

27. D. L. Stuehm and C. W. Wilmsen, "Three Josephson Junction Interferometer," Appl. Phys. Letters 20, 456 (1972).

28. D. L. Stuehm and C. W. Wilmsen, "Critical Current Periodicity of Josephson Junction Interferometers," J. Appl. Phys. 43, 3588 (1972).

29. D. L. Stuehm and C. W. Wilmsen, "Josephson Junction Interference Gratings," J. Appl. Phys. 44, 2881 (1973).